AD-A135 061 MAXIMUM LIKELIHOOD RECONSTRUCTION IN EMISSION TOMOGRAPHY WITH TIME-OF-FLI..(U) MASSACHUSETTS INST OF TECH CAMBRIDGE STATISTICS CENTER L KAUFMAN ET AL. 1/1

UNCLASSIFIED OCT 83 TR-ONR-33 N00014-75-C-0555 F/G 12/1 NL

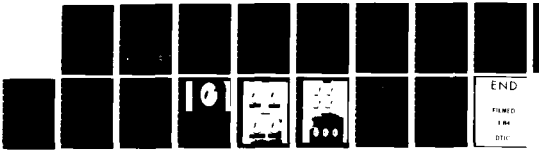

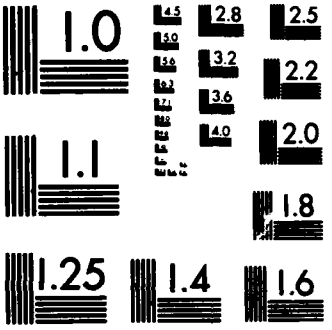

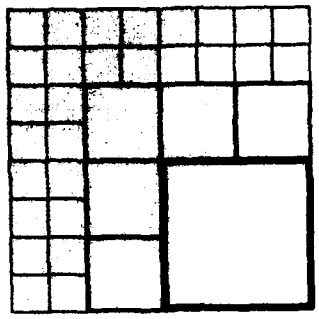

STATISTICS CENTER

Massachusetts Institute of Technology

77 Massachusetts Avenue, Rm. E40-111, Cambridge, Massachusetts 02139 (617) 253-8722

MAXIMUM LIKELIHOOD RECONSTRUCTION IN EMISSION TOMOGRAPHY WITH TIME-OF-FLIGHT INFORMATION: A LIMITED STUDY

BY

L. KAUFMAN (*), S. MORGENTHALER (#) AND Y. VARDI (*)

MASSACHUSETTS INSTITUTE OF TECHNOLOGY (#)

AND

BELL LABORATORIES (*)

TECHNICAL REPORT NO. ONR 33

OCTOBER 1983

PREPARED UNDER CONTRACT

N00014-75-C-0555 (NR-609-001)

FOR THE OFFICE OF NAVAL RESEARCH

Maximum Likelihood Reconstruction in Emission Tomography with Time-of-Flight Information: A Limited Study

L. Kaufman (*), S. Morgenthaler (#) and Y. Vardi (*)

Massachusetts Institute of Technology (#)

and

Bell Laboratories (*)

ABSTRACT

The maximum likelihood reconstruction for positron emission tomography (PET) and its use in connection with time-of-flight (TOF) tomography are reviewed and the issue of trade-off between information and data (that is, time of flight information vs. additional coincidence count data) is explained. The maximum likelihood technique is then used to qualitatively assess this trade-off by means of visually comparing reconstructions. Specifically, we use computer simulation to generate data of PET experiments with a fixed emission density λ and with varying amounts of TOF information and total coincidence count data. We then use the maximum likelihood technique to reconstruct λ on the bases of these data sets and the different reconstructions are displayed and compared.

Keywords and phrases: image reconstruction, poisson likelihood, simulation, subtubes

1. INTRODUCTION

In positron emission tomography (PET), a compound containing a radioactive isotope is introduced into the body and forms an unknown emitter density $\lambda(x, y, z) \geq 0$, determined by the body's metabolism. Positrons are then emitted according to a Poisson process with rate $\lambda(x, y, z)$. Upon emission, each positron finds a nearby electron with which to annihilate and as a result a pair of X-ray photons fly off the point of annihilation, at the speed of light, in opposite directions along a line with random orientation in space.

A scanner, which consists of an array of discrete detector elements mounted on a ring, surrounds the body and the two photons are detected in coincidence by a pair of detector elements defining a cylindrical volume, to be referred to as a detector tube, or simply a tube. The data acquired during a PET scan is then, $n^*(d)$ $d = 1, \ldots D$, the total number of coincidences counted in each of the D detector tubes, and with the use of an appropriate mathematical algorithm the emission density, λ, is estimated on the basis of these data.

Most PET scanners use time-windowed coincidence detectors to determine the tube in which the annihilation event took place, but recent improvements in high speed electronics and scintillation-crystal technology suggests that in the near future measurement of the small differential in

time of arrival (at the detectors) of the annihilation photons will be possible. This time-of-flight differential can then be used to estimate the position of the point of annihilation along the tube. For instance, consider the situation described in Figure 1 where an annihilation is counted in detector tube $d = (3, 67)$ (that is, the tube defined by the 3-rd and the 67-th detectors) and suppose the photon hitting the 67-th detector arrived there Δ time units after the arrival of the photon at the 3-rd detector, then simple algebra shows that the position X of the annihilation along the tube (3, 67) is

$$x = \frac{L_{3,67}}{2} + \frac{c}{2}\Delta \qquad (1.1)$$

units of distance from the 67-th detector and $(L_{3,67}-x)$ units of distance from the 3-rd detector, where $L_{3,67}$ denotes the tube's length and c is the speed of light.

Figure 1 here

In an ideal situation we would be able to measure the time-of-flight differentials, Δ, to perfect accuracy which in turn would enable us to determine the exact locations (up to the granularity of the tubes) of all the recorded annihilation events; in that case there is no need for any mathematical or statistical reconstruction technique. In

reality, however, Δ cannot be measured with perfect accuracy and measurement errors in the time domain are translated, via (1.1), into errors in the space domain. For example, 300 picoseconds in timing resolution correspond to 4.5 cm in spatial resolution. The timing resolution, i.e. the accuracy with which the TOF differential, Δ, can be measured, is a characteristic of the scanner and it depends on the detector materials and the electronic instrumentation. In positron tomography with TOF information the data then consists of the tube counts, $n^*(d)$, and the TOF differentials $\Delta_{d,1}, \ldots, \Delta_{d,n^*(d)}$ for the recorded coincidences in each tube d, $d = 1, \ldots, D$.

Knowledge of the timing resolution of the scanner then enables us to convert the time events, Δ's, into position events in some statistically sound way and to estimate the emission density λ. In situations where the detector materials are such that the timing resolution is too low to be of practical use, the estimation of λ is based only on the total number of coincidences, $n^*(d)$, counted in each tube d, $d = 1, \ldots, D$, and it does not take into account any TOF information; this situation is referred to as PET without TOF information, or simply as PET (no adjuncts). Presently, most PET instruments in use do not measure TOF information; nevertheless, at least four devices that would measure it are currently under intensive development and a considerable research effort is going into improving positron tomography resolution by incorporating TOF information.

TOF information, however, is only one factor in determining the image resolution for a given scanner design. Another important factor is the detection efficiency, which is the probability that a pair of annihilation photons arriving at the scintillation detectors do indeed record a coincidence (in the right tube). Note that the detection efficiency is a characteristic of the detector material as well as the material separating the detectors (because the high energy photons can cross, diagonally, through the neighboring detectors). Clearly, for a given dosage of the radionuclide, the total number of coincidences counted,

$$N^* = \sum_{d=1}^{D} n^*(d) ,$$

is higher for detectors with higher efficiency, and so they will have more data to estimate the emission density λ. This, in turn, implies that the higher the detection efficiency the higher the resolution of the reconstructed emission density. Here we assume, of course, that all other aspects influencing the reconstruction such as the type and dosage of the radionuclide, the scanner design, the mathematical algorithm used for reconstruction, etc. are fixed.

At present, all the detector materials with high timing resolution which have been considered for TOF positron tomography (e.g. CsF, liquid xenon, BaF_2, and more) have

detection efficiency lower than that of materials used in no TOF tomography (mainly BGO crystals) and so, at this stage, the question whether TOF tomography would produce a better reconstruction of the emission density, λ, depends on the trade-off between TOF information and more coincidence data.

A limited effort in studying this trade-off is presented in this paper. Specifically, we use computer simulation to compare pictures of the reconstructed emission density, λ, obtained from PET without TOF information with those obtained from PET with TOF information. The material is organized as follows. In 2 we review the maximum-likelihood reconstruction (Shepp and Vardi, 1982) and discuss it in the context of TOF tomography. In 3 we use computer simulation of PET experiments and the maximum-likelihood reconstruction to assess the contribution of TOF information to improved resolution, by varying the amount of TOF information across experiments, but leaving other factors important for the reconstruction fixed. In 4 we summarize our (qualitative) findings, suggest some directions for future research, and give some bibliographic notes.

2. MAXIMUM LIKELIHOOD RECONSTRUCTION OF THE EMISSION DENSITY

2.1. NO TOF INFORMATION

Although the underlying emission processes is a continuous Poisson process, it is convenient, for mathematical simplicity as well as displaying purposes, to discretize it. Thus we assume a fine grid of, say, B pixels overlaid on the source of emission (the brain, say,) and suppose that the number of emissions from pixel b, say n(b), is a Poisson random variable with parameter $\lambda(b)$, $b = 1, \ldots, B$. Since the pixels are disjoint the n(b)'s are independent. If it were possible to monitor the n(b)'s then the maximum likelihood (ML) estimate of $\lambda(b)$ would have been n(b). However, the data available to us is not n(b), $b = 1, \ldots, B$, but rather $n^*(d)$ = total number of emissions detected in tube d, $d = 1, \ldots, D$. If we let

$p(b, d) \triangleq$ probability that an emission from pixel

b is detected in tube d , (2.1)

then $n^*(d)$ is a Poisson variable with mean

$$\lambda^*(d) \triangleq \sum_{b=1}^{B} \lambda(b)p(b, d) \ . \qquad (2.2)$$

Furthermore, because thinning of Poisson processes gives rise to independent Poisson processes, the $n^*(d)$'s are mutually independent. The likelihood of the data is then

$$L(\lambda) \equiv P(n^*|\lambda) = \prod_{d=1}^{D} e^{-\lambda^*(d)} \frac{\lambda^*(d)^{n^*(d)}}{n^*(d)!} . \qquad (2.3)$$

For mathematical convenience it is simpler to maximize (2.3), with respect to $\lambda(1), \ldots, \lambda(B)$, under the assumption that

$$\sum_{d=1}^{D} p(b, d) = 1, \qquad b = 1, \ldots, B . \qquad (2.4)$$

Note that if (2.4) does not hold, then by defining

$$\theta(b) = \lambda(b)p(b, \cdot)$$

$$q(b, d) = p(b, d)/p(b, \cdot)$$

where

$$p(b, \cdot) = \sum_{d=1}^{D} p(b, d) ,$$

we have

$$\lambda^*(d) = \sum_{b=1}^{B} \theta(b)q(b, d)$$

so that we can reexpress the likelihood function in terms of $\theta(1), \ldots, \theta(B)$ and the constants $q(b, d)$'s (replacing the original constants $p(b, d)$'s), but now the $q(b, d)$'s satisfy

$$\sum_{d=1}^{D} q(b, d) = 1$$

as required in (2.4). If $\hat{\theta} = (\hat{\theta}(1), \ldots, \hat{\theta}(B))$ is the maximum likelihood for the transformed variables, $\hat{\lambda} = (\hat{\theta}(1)/p(1, \cdot), \ldots, \hat{\theta}(B)/p(B, \cdot))$ is the ML estimate for the original variables. Thus there is no loss of generality in assuming that (2.4) holds. Note that in practice the

$p(b, d)$'s indeed have to be rescaled by dividing them by $p(b, \cdot)$, in order to compensate for different detection probabilities associated with different pixels. (The probability for an emission from pixel b to be detected at all, depends on the location of the pixel.)

Shepp and Vardi (1982) give an iterative scheme for maximizing (2.3), i.e. for deriving the ML estimate $\hat{\lambda} = (\hat{\lambda}(1), \ldots, \hat{\lambda}(B))$. The following is a summary of their method.

The Algorithm

1. Start with an initial estimate λ^{old}, say, satisfying $\lambda^{old}(b) > 0$, $b = 1, \ldots, B$.

2. If λ^{old} denotes the current estimate of λ, define a new estimate, λ^{new}, by

$$\lambda^{new}(b) = \lambda^{old}(b) \sum_{d=1}^{D} \frac{n^*(d)p(b, d)}{\sum_{b'=1}^{B} \lambda^{old}(b')p(b', d)} , \qquad b = 1, \ldots, B . \qquad (2.5)$$

(The algorithm could never lead to a positive/zero quotient; zero/zero is defined as zero.)

3. If the required accuracy for numerical convergence has been achieved then stop. Otherwise, return to step (2), with λ^{new} replacing λ^{old}. Note that numerical convergence can be determined either by testing whether

λ^{new} is sufficiently close to λ^{old}, or by testing whether the increment in the log likelihood,

$$L(\lambda^{new}) - L(\lambda^{old}) = \sum_{d=1}^{D} n^*(d) \left(\log \lambda^{*new}(d) - \log \lambda^{*old}(d)\right) , \tag{2.6}$$

is sufficiently small.

Some Properties of the Method

1. The log likelihood is concave and hence all its maxima are global maxima.

2. If B > D the maximum of L is not unique. (The necessary and sufficient condition for uniqueness is slightly more complicated; see Vardi, Shepp and Kaufman (1983)).

3. The algorithm converges to a point of maximum likelihood, $\hat{\lambda}$, and the convergence is monotone, in the sense that

$$L(\lambda^{old}) < L(\lambda^{new}) \tag{2.7}$$

unless $\lambda^{old} = \lambda^{new}$ in which case we have converged and $\lambda^{old} = \lambda^{new} = \hat{\lambda}$.

4. The algorithm is an instance of an EM algorithm (e.g. Dempster, Laird and Rubin 1977). It is also a gradient type algorithm in the sense that

$$\lambda^{new} = \lambda^{old} + \lambda^{old}_{diag} \left| \frac{\partial L(\lambda^{old})}{\partial \lambda(1)} , \ldots, \frac{\partial L(\lambda^{old})}{\partial \lambda(B)} \right| .$$

5. In each iteration we have

$$\sum_{b=1}^{B} \lambda^{new}(b) = N^* = \sum_{d=1}^{D} n^*(d) .$$

6. The method is generally applicable to any design geometry (single or multi-ring), to single or double photon emission tomography, and can incorporate TOF information. This flexibility of the method is usually obtained by redefining what we call a ``detector-tube'' as explained below.

2.2. TOF INFORMATION

In order to incorporate TOF information into the reconstruction, we can partition each tube d into m(d) subtubes $d_1, \ldots, d_{m(d)}$ and compute the detection probabilities $p(b, d_j)$'s. Both the m(d)'s and the detection probabilities, $p(b, d_j)$'s, depend only on the scanner geometry and the timing resolution which are characteristic of the scanner design, the detector material and the electronic circuity, but are independent of the patient or the isotope in use. Thus, for maximum efficiency those constants should be computed once and stored permanently so they can be recalled from memory during the reconstruction.

3. SIMULATION WITH LIMITED TOF INFORMATION - PICTURES COMPARISON

3.1. DESIGN OF THE SIMULATION

We assume a single detector ring of radius $\sqrt{2}$, with 128 equally spaced detectors mounted on it, and consequently our problem is reconstructing λ over a head section; a two dimensional reconstruction. The emission density, $\lambda(x, y)$, which is used to generate the data and which we want to reconstruct is as described in Figure 2; the nomenclature in the tomography literature for this quantity, or in general for the mathematical model which simulates a body section, is a "mathematical phantom" or simply a "phantom".

Figure 2 here

The phantom of Figure 2 is made up of 8 ellipses and is chosen as a simplified imitation of the brain metabolic activity where the skull metabolizes at a low rate of 0.1, while the ventricles, tumors, etc. metabolize at rates between 0.3 and 2.0. The region within which we look to reconstruct the phantom in a disc of radius 1 co-centered with the detector ring; we call it the patient circle. Overlaid on the patient circle (and circumscribed by the detector ring) is a 128x128 grid of display boxes that cover the square $|x|, |y| \leq 1$. In this setup the number of tubes that cross the patient circle is D = 65x64 (for all other

tubes $n^*(d) = 0$) and the number of display boxes, B, that overlap the patient circle is about $128^2\pi/4$. Since one of our main objectives is to investigate the trade-off between data and TOF information, we varied both components across experiments. Specifically we ran three separate sets of simulation experiments with total number of detected emissions, N^*, equal to 10^6, $6 \cdot 10^6$ and 10^7 in the first, second and third set of experiments, respectively. The sampling is done so that the distribution of emission points will agree with the Poisson model; the details are as in Shepp and Vardi (1982). The TOF information available for reconstruction, within each set of experiments is as described in the next two paragraphs on timing information and data. For each emission as it occurs a random line (uniformly distributed in angles) is chosen through the point of emission and the coincidence count, $n^*(d)$, in the tube defined by the two detector units which are intersected by that line is then incremented.

Timing Information. We partitioned each tube into an equal number, m, of subtubes. When m = 1 it means that we have no TOF information, when m = 2 it means that for each detected emission we know within which half of the tube it was originated, when m = 3 we know within which third of the tube the emission was originated, etc. Although this is not a very realistic situation, because in practice timing information is measured continuously as a time differential with a measurement error, we chose this simple minded model

for ease of programming.

Data. We have used the emission density described in Figure 1 to simulate the brain activity. For the experiments with 10^7 coincidence count we assumed no TOF information, so that m = 1; for the case of $6 \cdot 10^7$ coincidence count we assumed that m = 3, and for the case of 10^6 coincidence count we assumed m = 5. Also to see the effect of increased TOF information for a fixed number of coincidence count we generated additional data, and reconstructions, for 10^6 coincidences with m = 1 (no TOF information) and m = 3. The notation we use to describe the data, reconstructions, etc. are generally of the form a prefix followed by xMy, where x stands for the number of coincidence count in millions, and y stands for the TOF information parameter (number of subtubes in our case). Thus, DATA6M3, for example, denotes the tubes count for a PET experiment with 6 million detected emissions and TOF information of 3 subtubes; similarly RCN6M3 denotes the reconstruction based on such data, etc.

3.2. COMPARISON OF PICTURES

In order to qualitatively evaluate the contribution of TOF information to the image resolution we have to visually compare the photodisplays of the various reconstructions, all of which use the same phantom but different amounts of data and TOF information, as described before. First, however, we start with the ``histogram'' of the emission process based on 10^7 emissions (Figure 3); specifically this is

a photodisplay of the emissions grouped into the display pixels of the 128x128 grid. Note that this is the unobserved process that takes place in the brain.

Figure 3 here

Figure 3 can be taken as a benchmark for comparing our estimates of $\lambda(x, y)$ of Figure 2. The closer the estimate is to the histogram of Figure 3, the better it is. Figure 4a gives a ``histogram'' of the emission process based on $10^6$ emissions; comparing Figure 4a with Figure 3 we see that although they are basically very similar, Figure 4a is more ``granular'' because it is based on a substantially smaller number of emissions. Since the histogram of Figure 4a can be thought of as a reconstruction with a complete TOF information (sort of infinite number of subtubes) it makes sense to compare it with genuine reconstruction based on limited or no TOF information. Such a comparison is made with Figure 4b which gives the reconstruction based on 10^7 tube counts *and no TOF information*; i.e. RCN10M1. (*This reconstruction is based on 32 iterations of the algorithm (2.5).*)

Figure 4 here

It seems that HIST1M (or, alternatively RCN1Moo) is roughly equivalent in quality to RCN10M1 and both are very close to

HIST10M (Figure 3) in the sense that all the important details of the phantom are easily noticeable. Of course, complete TOF information is impossible to obtain, so that the histograms we display are of no operational value but rather of value as references, we continue to compare reconstructions with genuine TOF information. Specifically, Figure 5 compares RCN1M5 with RCN6M3 (both are based on 32 iterations of (2.5)).

Figure 5 here

RCN6M3 appears less ``granular'', cleaner, sharper, and more or less of the same quality as the right photodisplay of Figure 4. This is more easily observed in Figure 6 which includes RCN10M1 in the comparison of RCN1M5 and RCN6M3. In order to simplify the (inherently subjective) task of comparing the pictures, we displayed on the bottom row of Figure 6 an edge-enhanced picture of each reconstruction in order that the sharpness and granularity will be more apparent.

Figure 6 here

Both rows of Figure 6 show that RCN6M3 and RCN10M1 are very close in quality, and both are superior to RCN1M5. In order to visually judge the level of improvement in resolution

with increased TOF information we display in Figure 7 below, RCN1M1 (no TOF information), RCN1M3 and RCN1M5. Included, as a point of reference, is HIST1M (or alternatively RCN1Moo). The improvement in resolution can be seen by observing that the three small ``tumors'' (one in the center of the phantom and two below it) are becoming more pronounced as we move from RCN1M1 to RCN1M3 and then to RCN1M5.

Figure 7 here

4. FURTHER NOTES

4.1. SUMMARY AND FUTURE WORK

In this study we explored the merit of TOF emission tomography, an area of active research, by comparing reconstructions derived from various data sets which differ in their TOF information and total tube count. We did this using the maximum-likelihood method based on subtube measurements. Our qualitative findings point to the fact that TOF information indeed does improve resolution and as long as the detector efficiency is not too low, incorporating TOF information in the reconstruction process is a worthwhile thing to do. This seems to be the conclusion when we compare RCN6M3 with RCN10M1. Nevertheless, if the detector efficiency is low, then the added information in recording

TOF for each detected coincidence cannot compensate for the reduced total number of counted coincidences, and the resolution of the TOF system could actually be lower than that of a no TOF system with more efficient detectors. This is evident from the comparison RCN1M5 vs. RCN10M1. The experiment we have described, however, is limited in scope and one should not deduce yet any quantitative final conclusions from it. Its main limitations are:

(i) It is tied to a single specific phantom.

(ii) To simplify computations and programming efforts, the TOF information is not measured here by a continuous parameter that would measure, say, the standard deviation of the TOF measurement but rather by portions of tubes (1/m, where m is the number of subtubes).

In thinking of future research we hope that similar experiments based on a variety of phantoms together with more accurate representation of the timing resolution parameter would suggest a sufficiently good mathematical model that would give rise to a figure-of-merit for the trade-off between TOF information and total coincidence count. For the purpose of illustrating what we have in mind, consider the following (somewhat crude) heuristic model:

Let $\lambda(b)$, $b = 1, \ldots, B$, be the Poisson parameters, and let t denote the measurement period so that $n(b, t)$, the number of emissions from box b during the measurement period

$(0, t]$, is a Poisson variable with mean $\lambda(b)t$ (the correction for half life decay is easily handled, and will be ignored in this discussion). In previous sections we have neglected any specific reference to the measurement period $(0, t]$, because it was assumed fixed or indirectly expressed as the total tube counts n^*, which has a Poisson distribution with mean $t\Sigma\lambda(b)$. In analogy with the assumption that

$$n(b, t)|\lambda \sim \text{Poisson}(\lambda(b)t) \qquad b = 1, \ldots, B \quad \text{(independent)} \tag{4.1}$$

let us suppose, as a crude approximation, that the conditional distribution of $\hat{n}(b, t, \Theta)$ - the estimated number of emissions in box b during the measurement period $(0, t]$ and with timing resolution parameter Θ - given $n(b, t)$ is Gaussian with mean $n(b, t)$ and variance $n(b, t)f(\Theta)$, for some nonnegative real function $f(\Theta)$. (We rediscuss this assumption at the end of this subsection.) That is

$$\hat{n}(b, t, \Theta)|\{n(b', t);\ b' = 1, \ldots, B\} \sim \text{Gaussian}(n(b, t), n(b, t)f(\Theta))$$

$$b = 1, \ldots, B \quad \text{(independent)} \tag{4.2}$$

where the timing resolution parameter, Θ, varies in the range $[1, \infty)$, say, and $f(\Theta) \geq 0$. Here $\Theta = \infty$ is equivalent to a complete TOF information (e.g. number of subtubes, m, is ∞) and $\Theta = 1$ is equivalent to no TOF information (e.g. number of subtubes, m, is 1). In the context of this model one expects $f(\infty) = 0$, in which case (4.2) says that with

complete TOF information we can fully recover the data $n(b, t)$, and $f(1)$ to be some positive constant. The function $f(\theta)$ should therefore be monotone decreasing and tend to 0 as θ grows. From (4.1-2) we get that

$$E\ \hat{n}(b, t, \theta)/t = \lambda(b)\ , \tag{4.3}$$

$$VAR\ (\hat{n}(b, t, \theta)/t) = \lambda(b)(f(\theta)+1)/t\ . \tag{4.4}$$

An estimate of $f(\theta)$ on the basis of a single box, b say, with $n(b, t) > 0$ is

$$\hat{f}_b(\theta) = \left|\frac{\hat{n}(b, t, \theta)-n(b, t)}{\sqrt{n(b, t)}}\right|^2 \tag{4.5}$$

which from (4.1-2) has the distribution

$$f(\theta)\ (\text{Gaussian}\ (0, 1))^2$$

independently of b, with

$$E\ \hat{f}_b(\theta) = f(\theta) \quad \text{and} \quad VAR\ \hat{f}_b(\theta) = 2f(\theta)\ .$$

To get an estimate $\hat{f}(\theta)$ of $f(\theta)$ on the basis of the entire data we can average $\hat{f}_b(\theta)$ over all b's for which $n(b, t) > 0$. Note that using simulation experiments of the type we described in section 3 we can indeed estimate $f(\theta)$ using this method because $n(b,t)$ is known. Now, for an experiment with timing resolution parameter θ_0 and measurement period t_0 the ``resolution'' of the reconstructed image as measured by (4.4) is proportional to $(f(\theta_0)+1)/t_0$. To obtain the same resolution with the same phantom but with no TOF information (i.e. $\theta = 1$), the measurement period should be increased to

$$t_1 = \frac{f(1)+1}{f(\theta_0)+1}\ t_0\ .$$

Thus, the quantity

$$\eta(\theta) = \frac{\hat{f}(\theta)+1}{\hat{f}(1)+1}$$

could be taken as a figure-of-merit for the trade-off between TOF information and coincidence count data (which is linearly proportional, in expectation, to the measurement period). It satisfies

$$0 < \eta(\theta) \leq 1 \quad \text{for} \quad 1 \leq \theta < \infty$$

and its interpretation is that if $\eta(\theta_0) = .8$, say, then the total coincidence count data needed for reconstruction with TOF parameter θ_0, is about 80% of the total count needed without TOF information in order to achieve comparable resolution.

The model above makes several assumptions, that may not hold in practice. In particular (4.2) which implies that $\hat{n}(b, t, \theta)$ is an unbiased estimate of $n(b, t)$ and that it is independent of $n(b', t)$ for $b' \neq b$. Furthermore, the derived figure-of-merit, $\eta(\theta)$, may very well depend on the mathematical phantom in use. Thus we feel that further research should go into this problem and at this stage, this model should only be considered as an illustration of a possible line of attack for this problem. The simple minded approach expressed by (4.5) does not seem to do a good job. Reconstructions judged superior by subjective eye judgments, can in some cases lead to higher overall averaged value of (4.5). Before calculating a variability figure

like (4.5), it seems necessary to preprocess the pixel estimates in a way similar to eye-smoothing. Another important ingredient of any subjective judgement seems to be associated with how well the "tumors" are standing out. We probably have to incorporate this global property of the reconstruction into an averaged value of (4.5).

5. BIBLIOGRAPHICAL NOTES

Past development, current status and future directions of positron emission tomography are discussed in the recent review articles by Brownell et al. (1982) and by Ter-Pogossian et al. (1980). The articles give many references and they provide an excellent overview of the subject, including discussions on the clinical, biochemical, and other interesting aspects of PET. Image reconstruction techniques for TOF tomography are discussed in Snyder (1982b) and Snyder et al. (1981). These techniques are more cumbersome than the algorithm used here, and they require preprocessing of the TOF data prior to the mathematical reconstruction step; performance comparisons of the various algorithms, which differ in the mode of data preprocessing, are given on the basis of mathematical models. The question of performance gain due to timing information is briefly addressed in Snyder (1982a). Here the prediction in performance gain is based on mathematical models and no pictures

of reconstructions are displayed. The maximum likelihood reconstruction algorithm, (2.5), was first given by Shepp and Vardi (1982) who discuss the algorithm properties (end of section 2.1) and show that it is an EM algorithm (e.g. Dempster, Laird and Rubin, 1977) which implies the monotonicity property (2.7). Additional discussion can be found in Vardi, Shepp and Kaufman (1983). The concept of subtubes and the adaptability of the algorithm to TOF tomography were suggested in Shepp and Vardi (1982). These ideas were further pursued by Snyder and Politte (1983) who used the algorithm (2.5) with TOF data by replacing the pixels, b, with quantized positions, x, and subtubes, d, with quantized positions and quantized angles, (u, α), so that p(b, d) becomes p(x, (u, α)) which is then assumed to have a probability density of the form, $p_\lambda(x-u|\alpha)$, with λ being a parameter which reflects knowledge of the timing resolution. The Workshop on TOF Tomography (1982) is dedicated to PET with TOF information and it contains numerous papers that cover a broad range of topics in TOF tomography (biomedical motivations, systems under development, event detection, reconstruction algorithms, design consideration and data acquisition and processing). Papers which compare detector materials in terms of their detection efficiency and timing resolution are given in the workshop's publication by Derenzo (1982) and by McIntyre (1982). Specifically, TOF figures-of-merit for detector materials are defined and various detector materials are compared. In the context of our

paper here, the described characteristics of the detectors are useful for calibrating simulation experiments of the type that we described in 3, so that the assumed timing resolution and efficiency parameters are within practical range.

Acknowledgement

We wish to thank R. McGill for help with the display device, L. A. Shepp for useful conversations, and A. R. Wilks for providing some of the display software.

REFERENCES

Brownell, G. L., Budinger, T. F. Lauterbur, P. C. and McGeer, P. L., Positron Tomography and Nuclear Magnetic Resonance Imaging. Science, 5 February 1982.

Derenzo, S. E., Comparison of Detector Materials for Time-Of-Flight Positron Tomography. In Workshop on Time-Of-Flight Tomography (see reference below).

McIntyre, J. A. Plastic Scintillators for Time-of-Flight Tomography. In workshop on Time-of-Flight Tomography (see reference below).

Shepp, L. A. and Vardi, Y., Maximum Likelihood Reconstruction for Emission Tomography. IEEE trans. on Medical Imaging, October 1982.

Snyder, D. L. and Politte, D. G., Image Reconstruction From List-Mode Data in an Emission-Tomography System Having Time-Of-Flight measurements. IEEE trans. on Nucl. Sci. June 1983.

Snyder, D. L., What Performance Gain Does An Emission Tomography System Having Time-Of-Flight Measurements Offer? IEEE trans on Nucl. Sci., June 1982(a).

Snyder, D. L., Some Noise Comparisons of Data-Collection Arrays for Emission Tomography Systems Having Time-Of-Flight Measurements. IEEE trans. on Nucl. Sci., Feb. 1982(b).

Snyder, D. L., Lewis, J. T. and Ter-Pogossian, M. M., A Mathematical Model for Positron-Emission Tomography Systems Having Time-Of-Flight Measurements. IEEE Trans. on Nucl. Sci., June 1981.

Ter-Pogossian, M. M., Raichle, M. E. and Burton, E. S., Positron-Emission Tomography. Scientific American, October 1980.

Vardi, Y., Shepp L. A., Kaufman, L. A Statistical Model For Positron Emission Tomography. To appear in J. Amer. Statist. Assoc. (submitted in 1983).

Workshop on Time-Of-Flight Tomography. Published by the IEEE Computer Society (order no. 440) IEEE Catalog no. 82CH1791-3. 17-19 May, 1982. Washington University, St. Louis, Missouri 63110.

FIGURE CAPTIONS

Figure 1. An annihilation event occurring at a point X is being detected at tube d = (3, 67).

Figure 2. This is the phantom used in our computer simulation.

Figure 3. This is the ``histogram'', n(b), b = 1,..., B, of the 10^7 emissions drawn from the phantom of Fig. 1 at a rate proportional to $\lambda(x, y)$ at each point.

Figure 4. Comparing (a) HIST1M with (b) RCN10M1.

Figure 5. Comparing RCN1M5 with RCN6M3.

Figure 6. Comparing RCN1M5, RCN6M3 and RCN10M1.

Figure 7. Comparing reconstructions based on 10^6 detected emissions and different amounts of TOF information. (Clockwise from upper left: HIST1M, RCN1M1, RCN1M3, RCN1M5.)

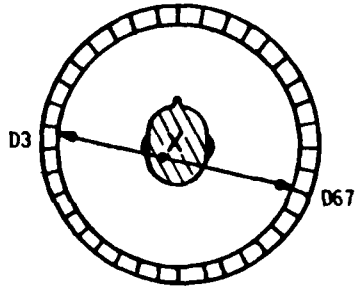

Figure 1

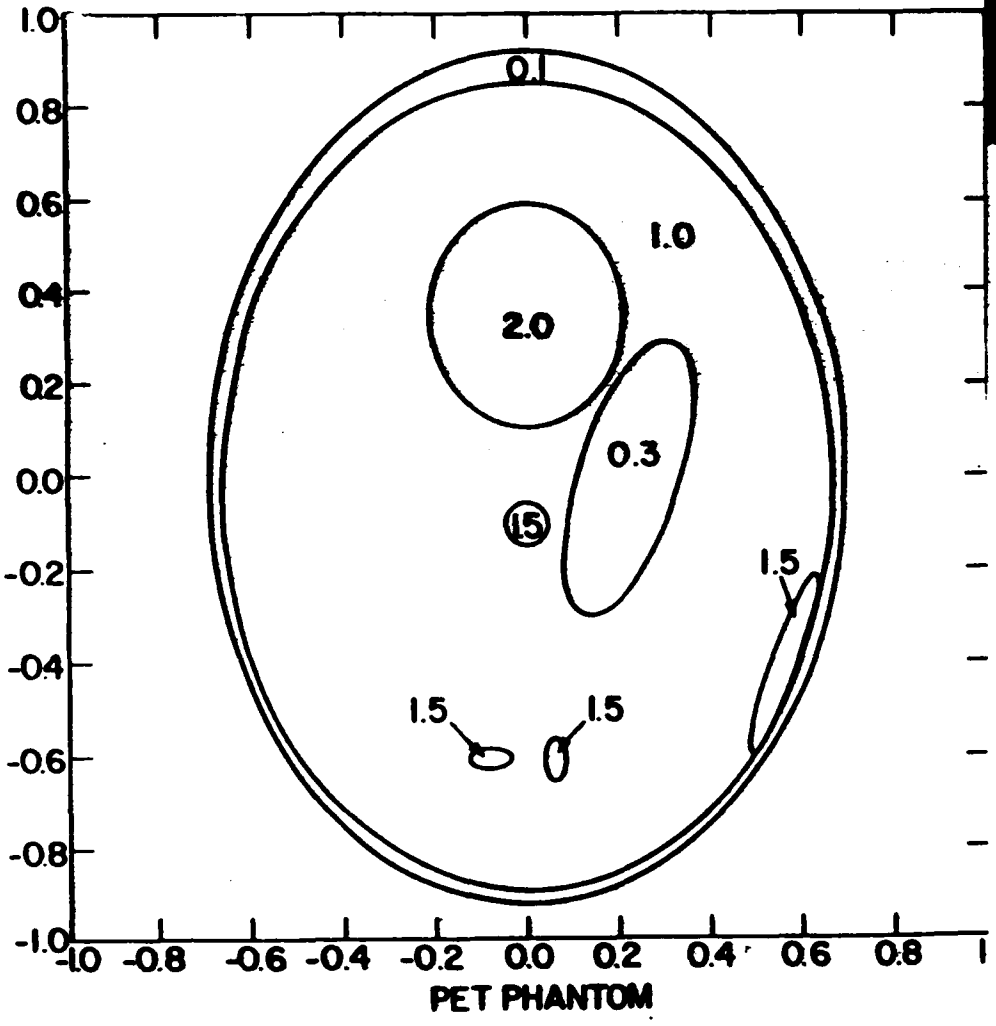
1.0
0.8
0.6
0.4
0.2
0.0
-0.2
-0.4
-0.6
-0.8
-1.0
-1.0 -0.8 -0.6 -0.4 -0.2 0.0 0.2 0.4 0.6 0.8 1
0.1
1.0
2.0
0.3
15
1.5
1.5
1.5
PET PHANTOM

Figure 2

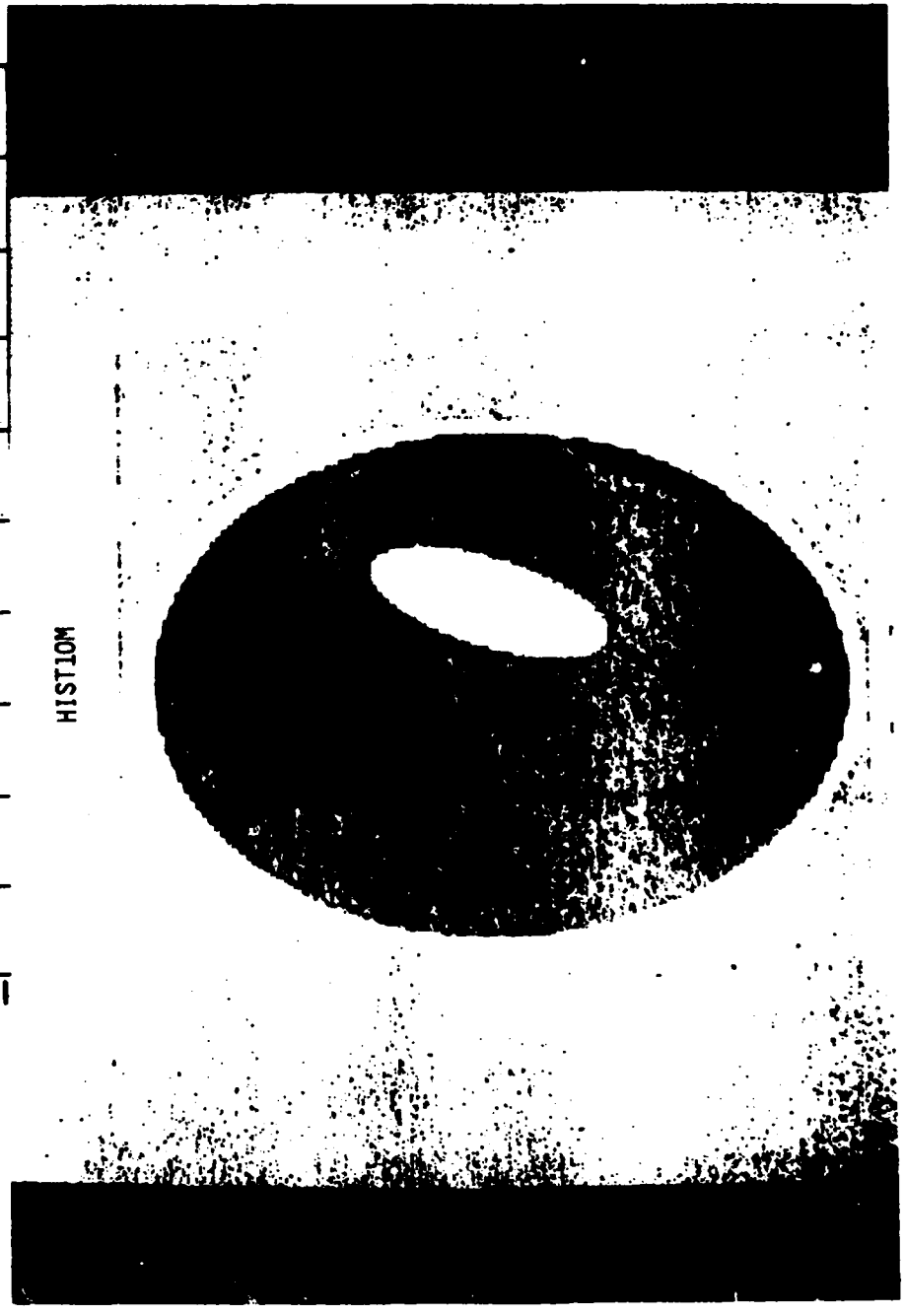
HISTIOM

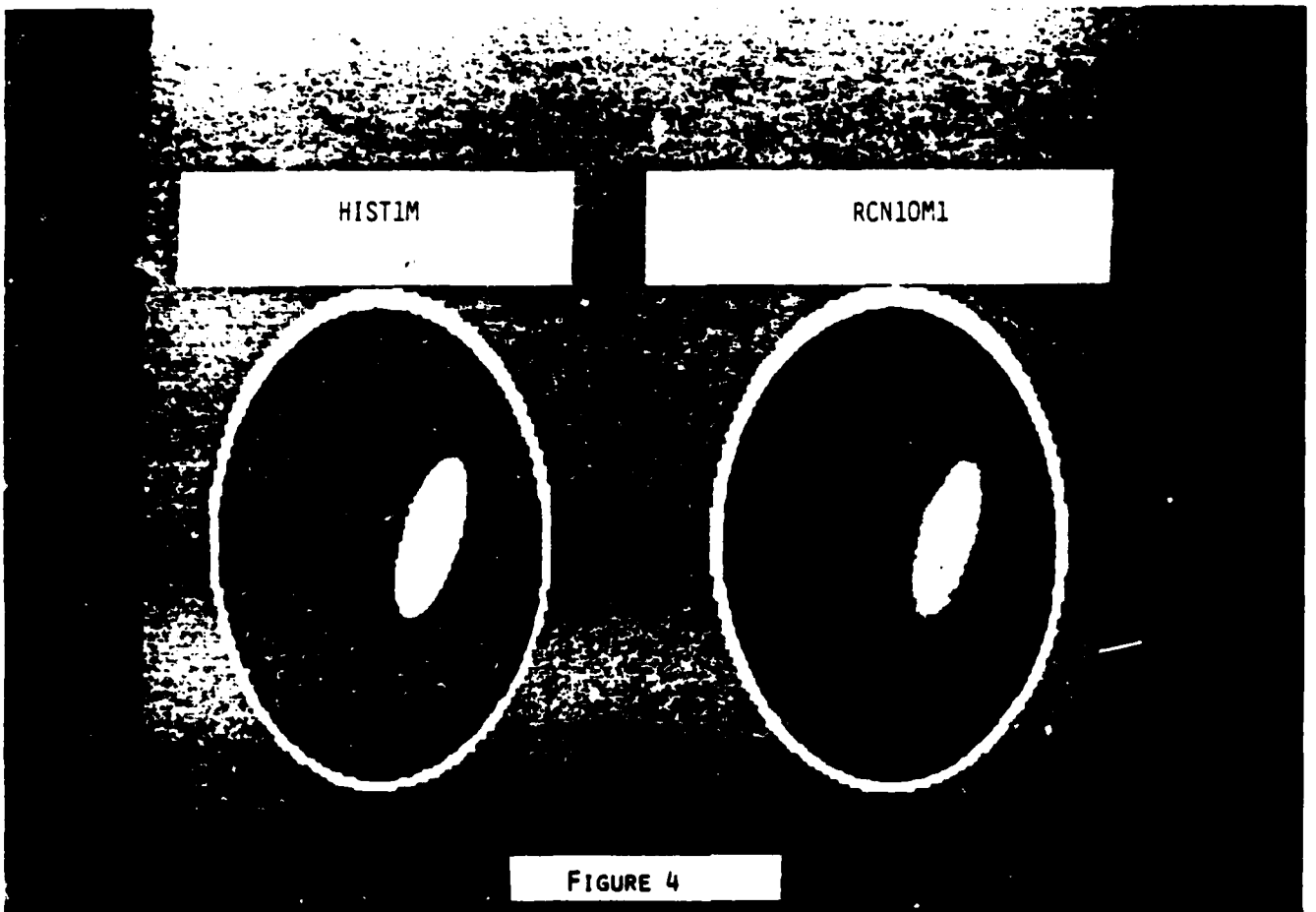

FIGURE 4

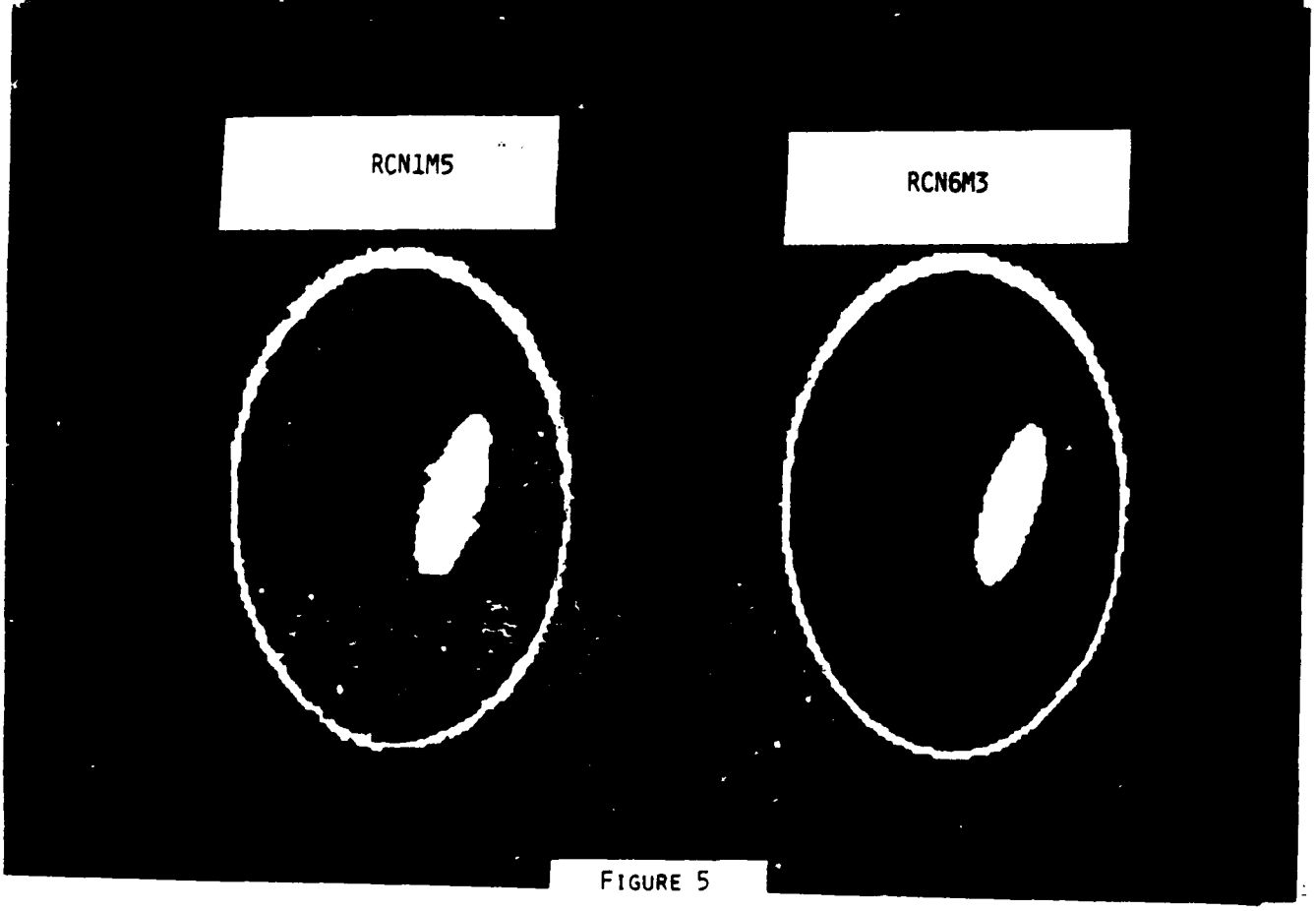

FIGURE 5

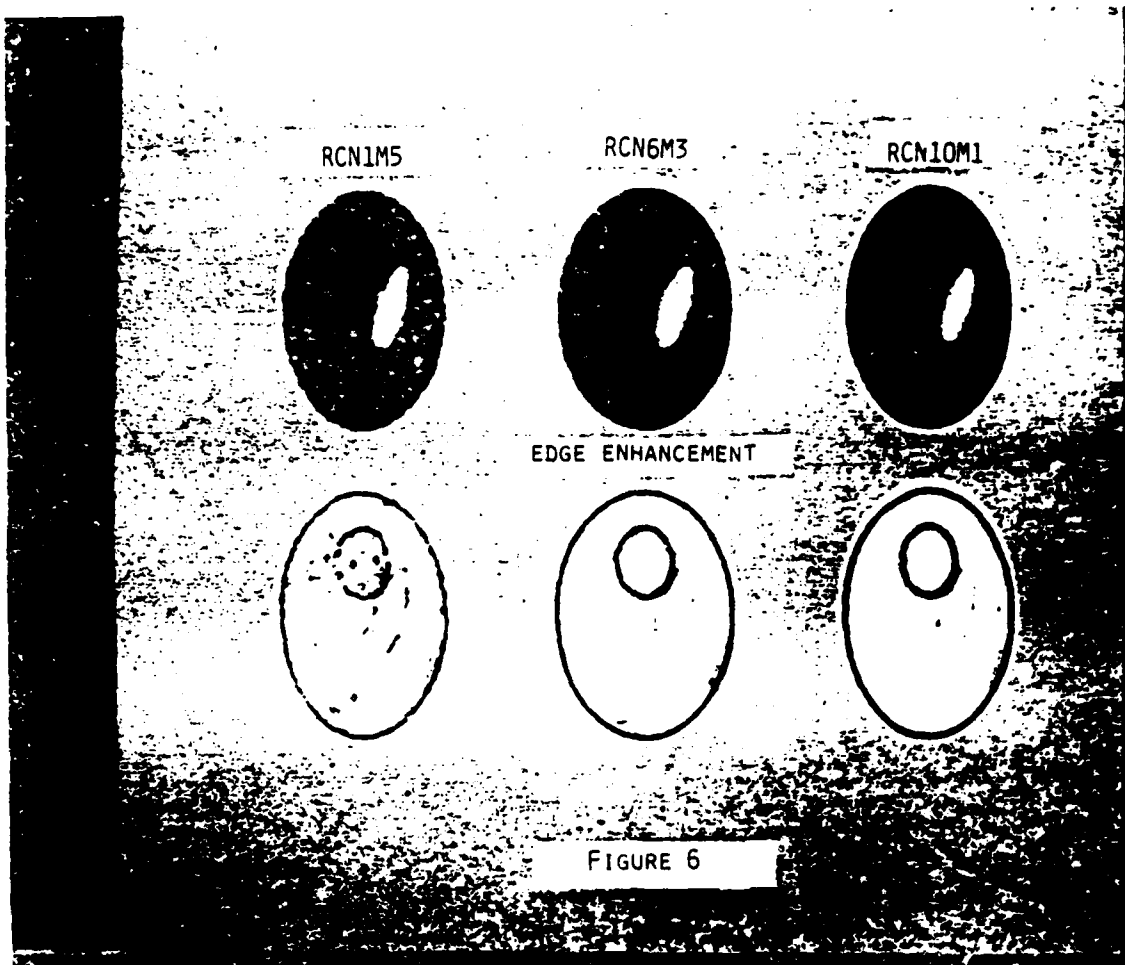

FIGURE 6

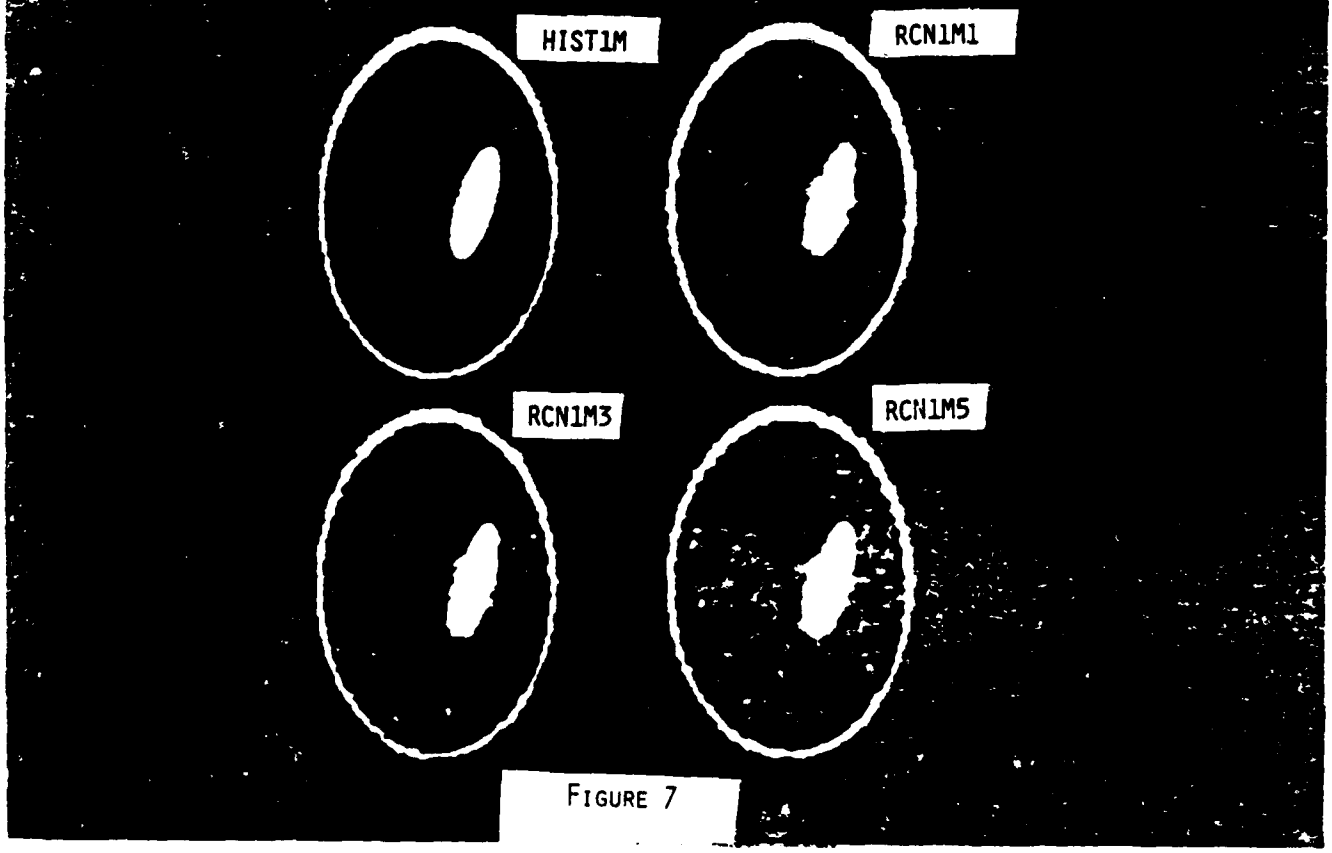

FIGURE 7

SECURITY CLASSIFICATION OF THIS PAGE (When Data Entered)

REPORT DOCUMENTATION PAGE	READ INSTRUCTIONS BEFORE COMPLETING FORM
1. REPORT NUMBER: 33	2. GOVT ACCESSION NO.: A136061
3. RECIPIENT'S CATALOG NUMBER:	
4. TITLE (and Subtitle): Maximum Likelihood Reconstruction In Emission Tomography With Time-Of-Flight Information: A Limited Study	5. TYPE OF REPORT & PERIOD COVERED: Technical Report
	6. PERFORMING ORG. REPORT NUMBER:
7. AUTHOR(s): L. Kaufman, S. Morgenthaler and Y. Vardi	8. CONTRACT OR GRANT NUMBER(s): N00014-75-C-0555
9. PERFORMING ORGANIZATION NAME AND ADDRESS: Statistics Center, Massachusetts Institute of Technology, Cambridge, MA 22217	10. PROGRAM ELEMENT, PROJECT, TASK AREA & WORK UNIT NUMBERS: (NR-609-001)
11. CONTROLLING OFFICE NAME AND ADDRESS: Office of Naval Research, Statistics and Probability Code 436, Arlington, VA 22217	12. REPORT DATE: October 1983
	13. NUMBER OF PAGES: 33
14. MONITORING AGENCY NAME & ADDRESS(if different from Controlling Office)	15. SECURITY CLASS. (of this report)
	15a. DECLASSIFICATION/DOWNGRADING SCHEDULE

16. DISTRIBUTION STATEMENT (of this Report)

This document has been approved for public release and sale; its distribution is unlimited

17. DISTRIBUTION STATEMENT (of the abstract entered in Block 20, if different from Report)

18. SUPPLEMENTARY NOTES

19. KEY WORDS (Continue on reverse side if necessary and identify by block number)

image reconstruction, poisson likelihood, simulation, subtubes

20. ABSTRACT (Continue on reverse side if necessary and identify by block number)

See reverse side

DD FORM 1 JAN 73 1473 EDITION OF 1 NOV 65 IS OBSOLETE

S/N 0102-LF-014-6601

Unclassified

SECURITY CLASSIFICATION OF THIS PAGE (When Data Entered)

The maximum likelihood reconstruction for positron emission tomography (PET) and its use in connection with time-of-flight (TOF) tomography are reviewed and the issue of trade-off between information and data (that is, time of flight information vs. additional coincidence count data) is explained. The maximum likelihood technique is then used to qualitatively assess this trade-off by means of visually comparing reconstructions. Specifically, we use computer simulation to generate data of PET experiments with a fixed emission density λ and with varying amounts of TOF information and total coincidence count data. We then use the maximum likelihood technique to reconstruct λ on the bases of these data sets and the different reconstructions are displayed and compared.

END

FILMED

1-84

DTIC